Dalton Transactions

Spectroelectrochemical Identification of Charge-Transfer Excited States in Transition Metal-based Polypyridyl Complexes

Journal:	*Dalton Transactions*
Manuscript ID:	DT-ART-09-2014-002849
Article Type:	Paper
Date Submitted by the Author:	16-Sep-2014
Complete List of Authors:	Brown, Allison; Michigan State University, Department of Chemistry McCusker, Catherine; Michigan State University, Department of Chemistry McCusker, James; Michigan State University, Department of Chemistry

Spectroelectrochemical Identification of Charge-Transfer Excited States in Transition Metal-based Polypyridyl Complexes

Allison M. Brown, Catherine E. McCusker,[†] and James K. McCusker[*]

Contribution from the Department of Chemistry, Michigan State University

578 South Shaw Lane, East Lansing, MI 48824

E-mail: jkm@chemistry.msu.edu

Abstract.

Identification of transient species is a necessary part of delineating the kinetics and mechanisms associated with chemical dynamics; when dealing with photo-induced processes, this can be an exceptionally challenging task due to the fact that spectra associated with excited state(s) sampled over the course of a photochemical event often cannot be uniquely identified nor readily calculated. Using Group 8 complexes of the general form $[M(terpy)_2]^{2+}$ and $[M(bpy)_3]^{2+}$ as a platform (where terpy is 2,2':6',2"-terpyridine and bpy is 2,2'-bipyiridine), we demonstrate how spectroelectrochemical measurements can serve as an effective tool for identifying spectroscopic signatures of charge-transfer excited states of transition metal-based chromophores. Formulating the metal-to-ligand charge-transfer (MLCT) excited state(s) as M^{3+}-L^{-}, the extent to which a linear combination of the spectra of the oxidized and reduced forms of the parent complexes can be used to simulate the characteristic absorptions of MLCT-based transient species is examined. Quantitative agreement is determined to be essentially unachievable due to the fact that certain transitions associated with the optically prepared excited states are either overcompensated for in the spectroelectrochemical data, or simply cannot be replicated through electrochemical means. Despite this limitation, it is shown through several illustrative examples that this approach can still be extremely useful as a qualitative if not semi-quantitative guide for interpreting time-resolved electronic absorption data of charge-transfer compounds, particularly in the ultrafast time domain.

Introduction

The ability to follow the transformation of chemical species over the course of a reaction is a necessary aspect of the study of chemical dynamics. Regardless of the nature or specifics of the reaction in question, a detailed understanding of the kinetics and mechanism(s) of a given process requires positive identification of the starting point, ending point, as well as any intermediate(s) that are sampled along the way.[1] In most cases, both the initial and final species can be independently prepared, isolated, and their spectroscopic and physical properties measured: this allows for the application of a wide range of techniques to monitor their decay and formation, respectively. In contrast, intermediates that are formed and disappear in the course of the chemical transformation can easily elude characterization due to short lifetimes and/or a lack of information as to how to correlate spectroscopic observables with their chemical origins. This latter situation is often encountered in photo-initiated processes where, upon irradiation, a molecule typically samples a number of electronic states as it evolves from the initially formed excited state to the endpoint of the photoreaction. Whereas the lowest-energy excited state of a compound might persist long enough to allow for definitive characterization, intermediate states critical for understanding the mechanism of excited-state evolution often possess sub-picosecond lifetimes. Recent advances in ultrafast methods have afforded an impressive array of new tools for acquiring spectroscopic information on such species,[2] but data interpretation nevertheless remains a significant challenge for the simple reason that one doesn't always know what to look for as a signature of a given excited state. The situation is particularly problematic for transition metal-containing chromophores due to the large number of electronic excited states endemic to this class of compounds;[3] their complexity is a double-edged sword insofar as it usually undermines efforts to gain reliable insights through computational methods.[4] This combination of factors often leads to considerable speculation concerning the mechanism(s) by which inorganic chromophores absorb and dissipate energy and is a significant hindrance to the further development of this class of compounds for various applications, including solar energy conversion strategies.[5]

Charge-transfer states represent one class of excited states for which the problem of *a priori* identification can be overcome, at least in principle. The idea underpinning this notion is the very nature of the charge-transfer state itself, namely as a photo-induced, charge-separated species. Eq 1 illustrates the basic formulation of the two most commonly encountered charge-transfer states in a generic tris-bidentate metal complex: metal-to-ligand charge-transfer (MLCT, eq 1a) and ligand-to-metal charge-transfer (LMCT, eq 1b).

$$[M^{n+}(L)_3] \xrightarrow{h\nu} [M^{(n+1)+}(L^{-})(L)_2] \quad (1a)$$

$$[M^{n+}(L)_3] \xrightarrow{h\nu} [M^{(n-1)+}(L^{+})(L)_2] \quad (1b)$$

In effect, light absorption results in an intramolecular charge redistribution between the metal and the ligand. Although the charge-transfer is never complete – the orbital overlap which is responsible for the non-zero oscillator strength of the charge-transfer transition necessitates a distribution of electron density between the metal and ligand in both the ground and excited state – the representation depicted in eq 1 is nevertheless a useful construct for characterizing the excited state as well as rationalizing its chemical reactivity.

One of the earliest examples of exploiting this connection between electrochemical charge-transfer states for excited-state characterization was the classic paper by Sutin and co-workers,[6] in which the absence of a feature associated with the radical anion of 2,2'-bipyridine was the first, definitive indication of the ultrafast nature of excited-state evolution in Fe(II) polypyridyl complexes. Since that report, other groups have demonstrated the utility of spectroelectrochemical data to enable the identification of charge-separated excited states in a variety of systems.[7] With this report, we wish to build upon this previous work and examine in some detail the advantages and limitations of spectroelectrochemistry as a tool for identifying, characterizing, and ultimately tracking the evolution of charge-transfer excited states. Due to their continued interest in the aforementioned solar energy conversion strategies, we will use polypyridyl complexes of Group 8 as a template for this discussion with a particular emphasis on the use of this construct for the interpretation of time-resolved electronic absorption data acquired on ultrafast time scales.

Experimental Section.

General. Spectrophotometric grade acetonitrile was obtained from Aldrich Chemical Co. and used without further purification. Tetrabutylammonium hexafluorophosphate ($TBAPF_6$) was obtained from Aldrich Chemical Co. and dried under vacuum prior to use. Bis(2,2':6',2"-terpyridine)iron(II) hexafluorophosphate ($[Fe(terpy)_2](PF_6)_2$),[8] tris(2,2'-bipyridine)iron(II) hexafluorophosphate ($[Fe(bpy)_3](PF_6)_2$),[8] bis(2,2':6,2"-terpyridine)ruthenium(II) hexafluorophosphate ($[Ru(terpy)_2](PF_6)_2$),[9] and tris(2,2'-bipyridine)ruthenium(II) hexafluorophosphate ($[Ru(bpy)_3](PF_6)_2$)[10] were synthesized according to literature methods. Composition and purity of each sample was confirmed using a combination of elemental analysis, electrospray ionization mass spectrometry (ESI-MS), and/or ^1H NMR spectroscopy.

Acquisition of Spectroelectrochemical Data. Four separate experiments were performed in order to enable comparison of the spectroelectrochemical results with the measured transient absorption spectra.

Ground-state absorption spectra. Ground state electronic absorption spectra were recorded on a Cary-50 UV-visible spectrophotometer in a 1 cm quartz cuvette. Extinction coefficients in spectrophotometric grade acetonitrile were measured using serial dilutions of an original solution.

Electrochemistry. Electrochemical measurements were carried out in an inert atmosphere glovebox (Vacuum Atmospheres) using a BAS CV-50W electrochemical analyzer. A standard three-electrode arrangement was used consisting of a Pt disk working electrode, a graphite rod counter-electrode, and a $Ag/AgNO_3$ reference electrode. Measurements were carried out in freeze-pump-thaw degassed spectrophotometric grade acetonitrile that was 0.1 M in $TBAPF_6$ as the supporting electrolyte. Cyclic voltammetry was used to determine the ligand reduction and metal oxidation potentials of each complex; $E_{1/2}$ values were calculated by taking the average of the anodic and cathodic waves for each process. The ferrocene/ferrocenium redox couple was used as an external reference for each sample.

Spectroelectrochemistry. UV-visible spectroelectrochemical experiments were performed in a dual-path length spectroelectrochemical cell (CH Instruments) in an Ar-filled glovebox (Vacuum Atmospheres). The 1 cm x 1 cm space on the top of the cell held the $Ag/AgNO_3$ reference electrode and platinum wire counter electrode while the platinum mesh working electrode was placed in the 1 mm x 1 cm path length bottom of the cell to electrolyze the solution while it was interrogated by light with a SI400 CCD spectrometer. Data were acquired on solutions identical to that just described for the electrochemical measurements, with the exception that solutions of each complex were adjusted to have absorbance values in the range of 0.7 ± 0.1 at the maximum of the lowest energy $^1A_1 \rightarrow {}^1$MLCT absorption peak. One 10 mL sample solution was prepared and a 1 mL aliquot of the stock solution was used to fill the sample cell for each oxidative or reductive experiment. A ground-state absorption spectrum was taken prior to the onset of bulk electrolysis; overpotentials of 100-200 mV relative to the first reductive and oxidative waves were applied to the static (i.e., not stirred) sample. Spectra were collected every 20-30 seconds for 20 minutes against a blank consisting of the solvent and electrolyte. The level of completion of the electrolysis varied slightly as a function of the overpotential used and the specific positions of the electrodes in relation to each other, but is estimated to be in excess of 90% for the data reported herein. Isosbestic points were monitored over the course of the electrolysis to ensure that no sample decomposition occurred. Each spectroelectrochemical measurement was repeated 3-4 times on independently prepared samples in order to ensure reproducibility and consistency in the data. A discontinuity seen in some spectra at 475 nm corresponds to an instrumental artifact due to the changeover between the deuterium and tungsten lamps of the SI400 CCD spectrometer.

Ultrafast time-resolved electronic absorption data. Transient absorption data were collected on a Ti:Sapphire-based regenerative amplified laser system, the details of and protocols for which are

described elsewhere.[11,12] Samples were dissolved in spectroscopic grade acetonitrile and the data acquired in 1 mm path length quartz cells. Full spectral traces were collected in steps of Δt = 30 fs in the 325-625 nm range. Each spectrum shown has been corrected for group velocity dispersion.

Results and Discussion.

All of the molecules discussed in this report are low-spin d^6 polypyridyl complexes and have qualitatively similar spectral features in their ground states. The visible region is typically dominated by an intense ($\varepsilon \sim 10^4$ M^{-1} cm^{-1}) absorption feature that is easily assigned as a $^1A_1 \rightarrow {}^1$MLCT transition; aromatic ligands such as bpy and terpy possess their own, ligand-localized $\pi \rightarrow \pi^*$ absorptions in the near-ultraviolet that are only slightly perturbed upon binding to metals such as Fe and Ru.[13,14] The MLCT excitation formally transfers an electron from a $d\pi$ orbital (t_{2g} in O_h symmetry) on the metal to an unoccupied π^* orbital of the ligand. As shown by Boxer[15] and Woodruff[16] in particular, this initial absorption in the specific case of $[Ru(bpy)_3]^{2+}$ creates a Franck-Condon state that can be formulated as $[Ru^{III}(bpy^-)(bpy)_2]^{2+*}$: subsequent dynamics leading to a localized, long-lived ^{3}MLCT excited state have been the subject of considerable debate over the years and is beyond the scope of the present study.[17] The exceedingly short lifetime of the charge-transfer manifold in Fe(II) complexes like $[Fe(bpy)_3]^{2+}$ has precluded detailed studies of this system until very recently.[18] Nevertheless, the more ionic nature of the bonding in an Fe(II) complex relative to a Ru(II) analog implies that a similar description for the initially formed absorptive state (i.e., $[Fe^{III}(bpy^-)(bpy)_2]^{2+*}$) is appropriate. It is presumed that descriptions for the charge-transfer manifolds of $[M(terpy)_2]^{2+}$-type complexes can be conceptualized in an analogous fashion, although chromophores of this class have not been studied as extensively.[4c]

Characterization of the nature of the excited state being sampled can be achieved by exploiting a variety of spectroscopic tools, at least in principle. The simplest of these from a technical perspective is emission spectroscopy, where both steady-state and time-resolved methods are relatively straightforward to implement; however, with the exception of certain Ir^{III} complexes in which the presence or absence of fine structure in the emission profile has been used to differentiate ligand-localized $^3(\pi^* \rightarrow \pi)$ emission versus a $^3\text{MLCT} \rightarrow {}^1A_1$ transition,[19] emission spectroscopy seldom reveals features that are chemically descriptive. Rate constants for radative and non-radiative decay (k_r and k_{nr}, respectively) can provide some information along these lines but mainly through comparisons to other known chemical systems. Time-resolved vibrational spectroscopies (e.g., infrared and resonance Raman) offer a level of chemical specificity that emission does not,[20] but these methods are not as widely implemented within the physical-inorganic community in part due to the more labor-intensive nature of these experiments. Time-resolved

electronic absorption spectroscopy, on the other hand, is widely available and can provide considerable insight into the chemical nature of a given excited state.

Time-resolved absorption data are typically acquired in a differential mode, that is, the excited-state absorption features are referenced to the ground-state absorption properties. This produces data in the form of a change in the absorbance of the chromophore (ΔA) as a function of time following photo-excitation. Assuming that the absorption spectra (both ground- and excited-state) can be approximated in terms of a superposition of contributions from the various components, we can sketch out a qualitative picture of the features we would expect to be associated with an MLCT state and in so doing provide a blueprint of what to look for in order to identify it in a transient measurement. If we look at the "product" in eq 1a, we can immediately infer that the MLCT excited state will be characterized by the complete absence of MLCT transitions due to the fact that the metal center is formally oxidized in the excited state relative to the ground state. At the same time, this oxidation will give rise to new absorptions in the form of ligand-to-metal charge-transfer transitions involving the ligand(s) that do not house the excited electron. With regard to the ligand(s), placement of an electron in the π^* orbital effectively creates the radical anion of the ligand, L^-, and should therefore produce absorption features reminiscent of that chemical species. Finally, absorptions characteristic of the ligand(s) not involved in the MLCT excitation will be present in the excited state spectrum but may be attenuated and/or shifted depending on how sensitive the ligand-localized transitions are to the oxidation state of the metal. Overall, the experimentally observed time-resolved differential spectrum will therefore reflect a superposition of the "negative" of the ground-state spectrum – the ground state is completely and instantaneously lost upon photo-excitation – and these new absorption features resulting from photo-induced charge redistribution within the chromophore.

Scheme 1 illustrates how one may begin to formulate an equivalent description of an MLCT excited state based on ground-state redox properties; for simplicity, a $[M(terpy)_2]^{2+}$ species is used as an example. To a first approximation, one can think of the MLCT excited state spectrum in terms of a combination of absorptions associated with the oxidized and reduced fragments of the chromophore, i.e., M^{3+} and L^-, respectively, in accordance with eq 1a. A list of spectroscopic components one can anticipate by formulating the MLCT excited state in this way is shown in Table 1. The (potentially) most diagnostic of these are absorptions associated with the reduced ligand, L^-: while their intensities and positions in the experimental spectrum may not match up precisely with the spectroelectrochemical data (vide infra), the fact that L^- is present if and only if one is sampling an MLCT excited state[21] makes the spectroscopic markers associated with this moiety *the single most easily identifiable signature(s) for a charge-transfer state.* Along the same lines, identification of LMCT absorption(s) can also be quite useful insofar as these

transitions require a change in the oxidation state of the metal center relative to the ground state in order to be manifest. As the discussion to follow will show, their utility can sometimes be compromised by their (relatively) weak intensity coupled with the fact that they often appear at lower energy than the ground-state MLCT and can therefore be obscured by incomplete correction for excited-state emission and/or additional absorptions associated with L^- (vide infra).

Surprisingly, the least useful diagnostic tends to be the loss of ground-state MLCT intensity (i.e., a bleach in the MLCT region). Although such a loss is consistent with what one expects for the MLCT excited-state spectrum – photo-induced charge-transfer does alter the oxidation state of the metal – it is not definitive for characterizing the nature of the excited state being sampled for two reasons. First, as mentioned above, the loss of *all* ground-state absorptions – including the MLCT band – is an inherent consequence following excitation of the molecule. A hypothetical chromophore whose excited state is devoid of absorption features would yield a differential absorption spectrum that will look exactly like the negative of the ground-state spectrum, including the loss of the MLCT feature. The bleach that would be experimentally observed in this circumstance thus provides absolutely no information as to the chemical nature of the excited state in question. More subtle – but ultimately more significant when dealing with the spectroscopy of transition metal complexes – is the fact that a variety of excited states exist in this class of compounds that would be expected to have lower oscillator strengths for their MLCT transitions than the corresponding ground state of the same molecule. For example, in the case of Fe(II) polypyridyl complexes like $[Fe(bpy)_3]^{2+}$, it is well established that $^1A_1 \rightarrow {}^1$MLCT excitation ultimately results in the formation of a $^5T_2$ ligand-field state as the lowest energy excited state of the compound.[18] This excited state is characterized by a increase in Fe-N bond length on the order of 0.2 Å relative to the ground state. Since the oscillator strength of a charge-transfer transition is in part a function of the extent of metal-ligand orbital overlap, the longer bond length in the $^5T_2$ state should result in a decrease in the intensity of the $^5T_2$-based MLCT, a fact that has been demonstrated experimentally.[22] A time-resolved differential absorption spectrum of this system will therefore reveal a bleach in the MLCT region when sampling this ligand-field state due to the fact the molar absorptivity of the $^5T_2 \rightarrow {}^5$MLCT transition is less than that of the corresponding ground-state absorption, but this would be qualitatively indistinguishable from what one would observe if the excited state was charge-transfer in nature. So, while a bleach of the MLCT feature can certainly be useful in conjunction with observations of L^- and/or LMCT features, it cannot be considered definitive in isolation.

Modeling MLCT Excited-state Spectra. The discussion above outlines the general features upon which one can focus when using spectroelectrochemical data to help identify MLCT excited states in transient spectra. We now take this a step further and attempt to quantify this by using the spectra of the

ground, oxidized, and reduced species to calculate the differential absorption spectrum of an MLCT excited state based on this simple picture. As a starting point, we can approximate the excited-state differential absorption spectrum, ΔA_{ex}^{sim}, according to equation 3,

$$\Delta A_{ex}^{sim} = (A_{ox} + A_{red}) \cdot \eta - 2 \cdot A_{gr} \cdot (1 - \eta) \quad (3)$$

where A_{ox}, A_{red}, and A_{gr} are the absorbances of the oxidized, reduced, and ground-state species, respectively, and η is a scaling factor that will be discussed in more detail in the following section. If we assume that (1) ligand-localized transitions (L_i^{loc}) are insensitive to the oxidation state of the metal, and (2) that metal-localized (i.e., ligand-field) transitions will be too weak to observed in the excited-state differential absorption spectrum of a charge-transfer chromophore, one obtains the following expression detailing contributions to ΔA_{ex}^{sim}:

$$\begin{aligned} \Delta A_{ex}^{sim} = & [(M^{3+} - L_1)^{LMCT} + (M^{3+} - L_2)^{LMCT} + (M^{2+} - L_1^-)^{MLCT} + (L_1^-)^{loc}] \\ - & [2 \cdot (M^{2+} - L_1)^{MLCT} + (M^{2+} - L_2)^{MLCT} + (L_1)^{loc}] \end{aligned} \quad (4a)$$

We can write an analogous description of the experimental differential spectrum of an MLCT excited state subject to the same assumptions, eq 4b:

$$\begin{aligned} \Delta A_{ex}^{\exp} = & [(M^{3+} - L_1^-)^{LMCT} + (M^{3+} - L_2)^{LMCT} + (L_1^-)^{loc}] \\ - & [(M^{2+} - L_1)^{MLCT} + (M^{2+} - L_2)^{MLCT} + (L_1)^{loc}] \end{aligned} \quad (4b)$$

Upon comparison of these two expressions, one can immediately identify several features for which there is a 1-to-1 correlation between the calculated, redox-derived spectrum and those that will be observed experimentally. As was alluded to in the preceding discussion, absorptions associated with the ligand radical anion present in the MLCT excited state are faithfully reproduced in the calculated differential absorption profile derived from spectroelectrochemical measurements: this reinforces the notion of these features as being of singular importance for the identification of charge-transfer excited states. In addition, a loss of absorptive cross-section from the neutral form of the ligand involved in the charge-

transfer transition (L_1^{loc}) is seen to correlate well in terms of net contributions to the bleach features of the experimental and calculated redox-derived spectrum.

The situation becomes more complex, however, when we begin examining the various charge-transfer features that will comprise the two spectra. First, we note that while a bleach in the MLCT region is anticipated in both the experimental and simulated spectra, the redox-based spectrum overcorrects for this in the case of the MLCT feature associated with L_1. While this does not negate the qualitative information associated with this component, it will have an impact on our ability to quantitatively correlate the two sets of data (vide infra). In terms of new absorptive features, the fact that L_1 is only present in its radical form in the experimental spectrum means that a M^{3+}-L_1 LMCT band observed in the spectrum of the oxidized chromophore will not have a counterpart in the MLCT excited-state spectrum. The same is true for an MLCT band we will expect to observe in the reduced species $(M^{2+}\text{-}L_1^{-})^{MLCT}$, since the oxidation state of the metal in the MLCT excited state is formally 3+. Finally, an LMCT state that is best formulated as $(M^{3+}\text{-}L_1^{-})^{LMCT}$ cannot be replicated using electrochemical methods. Its qualitative description is effectively the inverse of the MLCT ground-state absorption (i.e., $M^{3+}\text{-}L_1^{-} \rightarrow M^{2+}\text{-}L_1$), suggesting energetics comparable to the ground-state MLCT absorption. However, given that the time constant for intersystem crossing in this class of compounds typically exceeds 10^{13} s^{-1},[17a,18,23] the resulting change in excited-state spin multiplicity relative to the ground state will likely render such a transition too weak to be detected in the excited-state spectrum except at very early times. A summary of this analysis is provided in Table 2.

Comparative Analysis of Redox-based and Experimental Transient Spectra of $[M(L)_2]^{2+}$ Chromophores. The preceding discussion suggests that a quantitative match between the experimental differential absorption spectrum and one simulated through the use of spectroelectrochemical data is not going to be possible. At the same time, there are clearly several spectroscopic features common to both sets of spectra that can serve as the basis for definitive assignments of a given transient as originating from a charge-transfer excited state. We now examine this point further by considering the spectroscopic properties of $[M(terpy)_2]^{2+}$ (M = Ru and Fe) in fluid solution.

Figure 1 shows the spectra for the ground state, oxidized, and reduced forms of $[Ru(terpy)_2]^{2+}$. The ground state transitions have been identified previously for this class of compounds.[13] High-energy absorptions around 310 nm (not shown) are easily assigned to $\pi \rightarrow \pi^*$ transitions of the neutral ligand. The absorption envelope in the mid-visible region – including the very distinctive band centered at 475 nm – corresponds to the MLCT absorption(s) of the compound. In contrast to the simplified description of the previous discussion, the data clearly reveal the presence of several overlapping transitions in this region. A detailed description of these bands – all of which are MLCT in nature – is beyond the scope of

this study but can be gleaned from time-dependent DFT calculations.[24] Upon oxidation, we can see that there is a dramatic attenuation of absorptions in the visible due to the conversion of Ru^{2+} to Ru^{3+} and the concomitant loss of all MLCT transitions. We note a slight bathochromic shift in the ligand-localized bands in the ultraviolet, but the modest nature of this change serves to validate our approximation that ligand-localized bands are (relatively) insensitive to the oxidation state of the metal. Although it is tempting to ascribe the weak bands in the 400 – 500 nm region as the LMCT expected for $[Ru(terpy)_2]^{3+}$, the possibility of incomplete oxidation in the bulk electrolysis of the sample precludes a definitive assignment in this regard. The main diagnostic piece of information from the oxidative portion of the equation, therefore, is the attenuation of absorptive cross-section in the region of the MLCT ground-state transition(s).

Reduction gives rise to much more substantive changes in the spectrum. Retention of some of the MLCT oscillator strength is evident, particularly by the persistence of the sharp feature near 475 nm, consistent with the fact that the reduced species still possesses both Ru^{2+} and a neutral terpy ligand. More significant is the appearance of new features both in the near-ultraviolet (350 – 400 nm) and red of the main MLCT band (500 – 600 nm). These bands are only present upon formation of the reduced chromophore and can therefore be immediately assigned to the radical anion of terpy; The fact that this species exhibits such strong features in readily accessible regions of the spectrum coupled with its unique association with the charge-transfer state underscores its utility as a diagnostic for the characterization of MLCT excited states in this class of compounds.

In order to complete the modeling of the photoexcited species, the calculated excited state is used in the equation for the difference spectrum as shown in equation 5,

$$\Delta A_\lambda = (\varepsilon_{ex} - \varepsilon_{gr})_\lambda \cdot b \cdot [C]_{gr} \cdot \eta \qquad (5)$$

where ΔA_λ is the change in absorbance at wavelength λ, ε_{ex} and ε_{gr} are the molar extinction coefficients for the excited and ground states, respectively, b is the path length, and $[C]_{gr}$ is the concentration of the sample. In the transient absorption experiments, the percentage of excited state formed is far less than 100% and varies due to factors such as pump power, pump beam size, and pump/probe overlap: this must be taken into consideration in the calculated difference spectrum in order to properly weight the relative contributions of the ground- and excited-state features to the observed spectrum. A factor η, which can range from 0 to 1, is therefore included in the expression for ΔA_λ, and while this formally reflects the

percentage of excited state formed (i.e., the fractional contribution of the excited state to the differential spectrum – and hence its presence in eq 3), in practice this is more properly viewed as a scaling term that is varied in order to obtain the best overall match between the calculated and experimental spectrum. Figure 2 shows the calculated difference spectrum of $[Ru(terpy)_2]^{2+}$ from spectroelectrochemistry along with the experimental difference spectrum from a transient absorption measurement. Using a value of 0.3 for η, one obtains reasonable agreement between the calculated and experimental differential spectrum of this compound. The loss of MLCT absorption is well represented, but more significant are the absorptions in the near-UV and at low energy, both of which are reproduced in the calculated redox-based spectrum. These features in the experimental spectrum are thus easily ascribed to transitions associated with $terpy^-$ and provide unambiguous evidence that the excited state being sampled in the time-resolved measurement is indeed MLCT in nature. The fact that the agreement is only qualitative – better in some regions than others – is a reflection of the discussion in the preceding section, namely that there are certain disconnects between what the calculated redox-based spectrum will provide and what is going to be present experimentally. Nevertheless, the level of qualitative agreement demonstrated by Figure 2 is sufficient to enable reliable conclusions to be drawn.

Ruthenium polypyridyl complexes represent one of the most widely studied classes of inorganic chromophores. It is well established that the lowest energy excited states in these systems are MLCT in nature; in these cases, the spectroelectrochemical data just described are more useful in terms of assignment of specific features rather than determining the overall character of the excited state.[25] The real advantage of the approach outlined above lies in the study of systems whose excited-state dynamics involve sampling states that are not charge-transfer, more specifically in systems for which the initially excited charge transfer state decays to other types of excited states on the ultrafast time scale. This is seldom encountered in complexes of second- and third-row transition metals because of the intrinsically large ligand-field strength endemic to such systems,[3] but complexes of the first transition series will almost always fall into this category due to the fact that low-lying ligand-field excited states can serve as efficient non-radiative decay pathways for initially formed MLCT states.[18,26] Understanding the dynamics of this conversion is therefore critically important from the perspective of chromophore design, particularly with regard to photo-induced electron transfer chemistry where the redox-active nature of the charge-transfer state needs to be leveraged. Identification of a spectroscopic tag for a charge-transfer state in this class of compounds would allow for definitive characterization of this first step in the conversion of light to chemical energy.

Spectroelectrochemical data acquired on $[Fe(terpy)_2]^{2+}$ are shown in Figure 3. These data and illustrate the progression of the electronic spectra as the parent compound is converted to its oxidized and

reduced forms and thus provide an indication as to what that spectroscopic tag might look like. As was the case with $[Ru(terpy)_2]^{2+}$, we see complete attenuation of oscillator strength in the mid-visible concomitant with oxidation, consistent with the conversion of Fe^{2+} to Fe^{3+} and loss of the MLCT chromophore. At the same time, we note the growth of a new, broad feature centered at ca. 700 nm that is easily assigned as an LMCT band associated with $[Fe(terpy)_2]^{3+}$. This feature, although still very weak relative to the MLCT band of the Fe^{2+} complex, is much more pronounced in this compound as compared to the Ru analog (Figure 1, middle). In addition, the fairly clean isosbestic at ~650 nm (as well as the one at ~420 nm) underscores the stability of the oxidized form of the compound, a trait that we have found to be a fairly common characteristic of Fe-polypyridyl complexes but not encountered as frequently in the case of Ru^{2+}.[27] The fact that this LMCT absorption occurs so far to the red makes it an excellent potential probe for electron transfer dynamics of this class of compounds. The growth of absorptions in the blue and near-UV regions are more difficult to assign, that is, whether they are LMCT bands involving higher energy orbitals of the ligand versus shifts in the ligand-localized $\pi \rightarrow \pi^*$ due to oxidation of the metal. For the purposes of identifying a transient spectrum as charge-transfer in origin, however, the inability to differentiate between these two possibilities from these data turns out to be of little consequence (vide infra).

Although spectral changes associated with the oxidation of $[Fe(terpy)_2]^{2+}$ are pronounced, they are not nearly as dramatic as what occurs upon formation of $[Fe(terpy^-)(terpy)]^+$ (Figure 3, bottom). As expected, we see retention of some MLCT oscillator strength in the mid-visible, however, the most significant features are associated with $terpy^-$: in both the red and, especially, in the blue and near-UV, there is a substantial increase in absorbance that together comprise distinct, unambiguous optical markers for the presence of the radical anion form of this ligand. It's interesting to note that the spectral features associated with both the oxidized and reduced forms of the compound reinforce each other, that is, net increases in absorption cross-section are observed in the same spectral regions for both the oxidized (LMCT) and reduced ($terpy^-$) contributions to a hypothetical MLCT excited-state spectrum. As will be shown below, this is an advantage when using these data to interpret transient spectra since spectral features associated with different components of the excited state will not offset each other in the manner one sees for the $[M(bpy)_3]^{2+}$ complexes to be discussed later.

As suggested by the data in Figure 2, the excited-state properties of $[Ru(terpy)_2]^{2+}$ are essentially defined by the ^{3}MLCT state that is formed following $^1A_1 \rightarrow {}^1$MLCT excitation.[28] Excited-state evolution of $[Fe(terpy)_2]^{2+}$ is going to be more complex due to the inversion of electronic state energetics alluded to previously. Since ligand-field states are not redox in nature – they correspond to multielectronic term states derived from various excited configurations among the d orbitals of the metal center – one can

anticipate that it should be possible to track the evolution from the charge-transfer to ligand-field excited-state manifold by focusing on features associated with $terpy^-$ and/or Fe^{3+}. The top panel of Figure 4 shows a plot of femtosecond time-resolved differential electronic absorption data acquired for $[Fe(terpy)_2]^{2+}$ following $^1A_1 \rightarrow {}^1$MLCT excitation. Although the strongest signal in terms of amplitude is the bleach of the MLCT band centered near 550 nm, the most important feature from a diagnostic perspective is the absorptive features in the blue and near-UV region (an expanded view of which is shown in the inset). Based on the reductive spectroelectrochemical data discussed above, these absorptions can be immediately ascribed to the radical anion of the ligand. The simulation of the differential spectra shown in the bottom panel of Figure 4 lends further support to this assignment, where the net absorbances at 350 and 400 nm derived from the superposition of the reductive and oxidative spectra bear a strong, semi-quantitative resemblance to the measured absorption profile acquired at a time delay of Δt = 200 fs. The correlation is not as good to the red side of the bleach, where one notes a significant difference between the calculated and experimental spectra in the 575 – 625 nm region. The reason for this discrepancy is not clear but may simply reflect the approximations made in constructing the anticipated redox-based signal. The agreement would be expected to improve for λ > 650 nm (vide supra) because of the lack of ground-state absorption at these longer wavelengths, but experimental limitations prevented the acquisition of data in this region of the spectrum.

In terms of kinetics, the inset in the upper panel of Figure 4 and the spectral snapshot at Δt = 1.5 ps highlights the rapid decay of the $terpy^-$ signal within the first picosecond of excited-state evolution. This is an unambiguous indication that the charge-transfer character of the excited state(s) of $[Fe(terpy)_2]^{2+}$ is completely lost on this time scale; the ~ 5 ns time-constant for ground-state recovery that has been documented for this compound is associated with relaxation from an excited state that is ligand-field in nature.[29] This conclusion is consistent with results that have been obtained on other Fe^{2+}-polypyridyl complexes and reflects the extraordinary rate at which this class of compounds non-radiatively decay from their initially formed excited states. It is important to note that the bleach in the MLCT region, while undergoing a slight modulation in shape, nevertheless persists through the loss of the $terpy^-$ signal. This illustrates the general guidelines discussed earlier, namely that attenuation of MLCT oscillator strength is not a sufficiently diagnostic marker for tracking the loss of charge-transfer character from the excited state. In the present case, there is a ~0.2 Å increase in the Fe-N bond length upon excited-state thermalization that results in a substantial decrease in metal-liagnd overlap and thus MLCT intensity relative to the ground state.

Comparative Analysis of Redox-based and Experimental Transient Spectra of $[M(L)_3]^{2+}$ Chromophores. An analogous approach can be employed for complexes of the general form

$[M(L_1)(L_2)(L_3)]^{2+}$ (e.g., $[Ru(bpy)_3]^{2+}$). Because of the presence of three ligands, there is an increase in the number of contributions to the both the redox-based and experimental differential spectra relative to what one sees for the $[M(L)_2]^{2+}$ species, as shown in eq 6a and 6b, respectively.

$$\begin{aligned}\Delta A_{ex}^{sim} = &[(M^{3+}-L_1)^{LMCT}+(M^{3+}-L_2)^{LMCT}+(M^{3+}-L_3)^{LMCT}+(M^{2+}-L_1^-)^{MLCT}+(L_1^-)^{loc}] \\ - &\ [2\cdot(M^{2+}-L_1)^{MLCT}+(M^{2+}-L_2)^{MLCT}+(M^{2+}-L_3)^{MLCT}+(L_1)^{loc}]\end{aligned} \tag{6a}$$

$$\begin{aligned}\Delta A_{ex}^{\exp} = &[(M^{3+}-L_1^-)^{LMCT}+(M^{3+}-L_2)^{LMCT}+(M^{3+}-L_3)^{LMCT}+(L_1^-)^{loc}] \\ - &\ [(M^{2+}-L_1)^{MLCT}+(M^{2+}-L_2)^{MLCT}+(M^{2+}-L_3)^{MLCT}+(L_1)^{loc}]\end{aligned} \tag{6b}$$

Despite the increase in the number of contributing species, the anticipated discrepancies between the redox-based and experimental differential spectra are exactly the same as was identified for the bis-tridentate system (Table 3). In terms of using the spectroelectrochemical data for interpreting time-resolved differential spectra, the same guidelines with regard to the preferred use of the ligand radical anion features being the most discriminating diagnostic for identifying charge-transfer character in the excited state should hold for this class of chromophores.

Figure 5 shows the ground-state, oxidized, reduced, and differential spectra for $[Ru(bpy)_3]^{2+}$ in CH_3CN solution. Comparing the ground-state and oxidized species, we again see loss of MLCT oscillator strength due to the conversion of Ru^{2+} to Ru^{3+}. The singly reduced species is dominated by transitions associated with the ligand radical in both the blue and red regions of the visible. The apparent shifting of the MLCT band maximum – which is more pronounced that what was observed for $[Ru(terpy)_2]^{2+}$ - occurs due to additional transitions that appear when the charge transfer transitions to neutral ligands are accompanied by transitions to the reduced ligand. In this system, the superposition of all the contributing chromophores is sufficiently displaced to both broaden and shift the overall absorption spectrum to the red more substantially that in $[Ru(terpy)_2]^{2+}$.

The more significant perturbations to the superposition spectra in $[Ru(bpy)_3]^{2+}$ have a discernable impact on the level of agreement between the redox-based and experimental differential spectra (Figure 5d). As mentioned above, there is no difference in the anticipated discrepancies when dealing with the tris complexes versus bis complexes: the number and type of transitions that are overestimated or not accounted for are the same. However, there is an obvious difference in the ability to model the excited-state spectrum of $[Ru(bpy)_3]^{2+}$ as compared to $[Ru(terpy)_2]^{2+}$. Whereas the calculated and measured

spectra for $[Ru(terpy)_2]^{2+}$ are in reasonable agreement across the entire spectrum, the redox-based spectrum fails to reflect the net contribution of bpy^- in the near-UV region for $[Ru(bpy)_3]^{2+}$. Empirically, the calculation must be either overestimating a negative contribution (i.e., a bleach) or underestimating a net absorption. Upon inspection of Table 3, we note that the calculated spectrum overestimates losses due to the M^{2+}-L_1 MLCT transition while not accounting for new transitions involving the M^{3+}-L_1^- species present in the excited state. The fact that the MLCT state being sampled experimentally is a triplet state (i.e., ^{3}MLCT) makes it unlikely that absorptive contributions from M^{3+}-L_1^- are significant since they will be spin-forbidden. A closer inspection of the calculated and photo-excited spectra with the ground state indicates that the origin of the poorer agreement in the case of $[Ru(bpy)_3]^{2+}$ can indeed be explained, at least qualitatively, by an overestimate of bleach contributions to the calculated spectrum. If one looks at the ground-state absorption spectra of $[Ru(bpy)_3]^{2+}$ and $[Ru(terpy)_2]^{2+}$, one notes that there is far less absorptive cross-section in the 350 – 400 nm region in $[Ru(terpy)_2]^{2+}$. This means that there will be no significant ground-state bleach contributions to either the calculated or measured differential absorption spectra in this region for $[Ru(terpy)_2]^{2+}$, and absorptions associated with $terpy^-$ will be superimposed on what will amount to an optically transparent background. In contrast, $[Ru(bpy)_3]^{2+}$ possesses far more optical density in this region in the ground state and will therefore be more susceptible to effects due to overcompensating the loss of these contributions. Identification of the charge-transfer nature of the excited state in this case therefore must rely not only a comparison of the calculated and experimental differential absorption spectra, but also on a direct comparison of the experimental data and the original spectroelectrochemical traces. When we do the latter for $[Ru(bpy)_3]^{2+}$, the correlation between the reductive and experimental spectra (Figures 5c and 5d, respectively) allows for an assignment of the differential absorptive feature at 370 nm as an absorption due to the presence of the radical anion of 2,2'-bipyridine in the excited state.

Another slight deviation between the calculated and experimental spectrum occurs on the red side of the main absorption bands. Since there are no strong absorptions in the ground state in this region, an explanation analogous to the one just described is not tenable. It's interesting to note that an underestimate of spectral amplitude in this region was also encountered for $[Ru(terpy)_2]^{2+}$ (Figure 2), suggesting that the LMCT absorption(s) in the excited state may be stronger in general than the spectroelectrochemical data are indicating. Regardless, the effect appears to be relatively minor.

A similar situation arises in the case of $[Fe(bpy)_3]^{2+}$ insofar as the redox-derived spectrum actually appears to be in better agreement with the experimental spectrum acquired at longer delay times (Figure 6). As with the analysis of $[Ru(bpy)_3]^{2+}$, the presence of ground-state absorptions in $[Fe(bpy)_3]^{2+}$ significantly compromises the level of agreement between the experimental and calculated spectra in the

region of bpy^- absorptions due to the overcorrection inherent from eq 6b. Upon comparison of the spectra at early time delays with the reductive spectroelectrochemical data, however, one can easily ascribe the net absorption features in the 350 – 450 nm region to bpy^- and the presence of a charge-transfer excited state immediately following photoexcitation. This spectral signature is seen to disappear with a time constant of < 100 fs, a clear indication that the MLCT excited state of this compound undergoes rapid conversion to another electron state(s) that does not contain the bpy^- chromophore. Although this has been established through the application of a variety of time-resolved techniques,[18] it is the ability to unambiguously identify features endemic to the charge-transfer excited states of these compounds that allow for these sorts of definitive conclusions to be drawn, even for systems as electronically complex as $[Fe(bpy)_3]^{2+}$.

One final point that should be noted is the change in the sign of the transient (i.e., absorption to bleach) concomitant with the loss of the bpy^- feature. The reason this is important can be gleaned from eq 5, which clearly shows that the sign of ΔA is wholly determined by the difference in molar extinction coefficients between the ground and excited states. Since ε_{gr} is constant, only a change in the magnitude of ε_{ex} can bring about a sign inversion of the differential signal, which in turn will only arise if there is a change in the electronic state being sampled.[30] In the case of $[Fe(bpy)_3]^{2+}$, then, the change in sign of $\Delta\varepsilon$ in the blue and near-UV regions of the spectrum provides evidence that the system is evolving from one electronic state(s) to another during the first few hundred femtoseconds following $^1A_1 \rightarrow {}^1$MLCT excitation, whereas spectroelectrochemical measurements inform as to the nature of that change. The combination of these pieces of information thus provides a sound basis for the interpretation of ultrafast transient absorption data and a more thorough understanding of excited-state dynamics in this class of compounds.

Acknowledgements. This research has been generously supported by the Division of Chemical Sciences, Geosciences, and Biosciences, Office of Basic Energy Science, Office of Science, U.S. Department of Energy under Grant No. DE-FG02-01ER15282.

References and Notes

†Present address: Department of Chemistry, North Carolina State University, Raleigh, NC 27695

1.) a) Espensen, J.H. *Chemical Kinetics and Reaction Mechanisms*, McGraw-Hill, New York, 1981. b) Moore, J.W.; Pearson, R.G. *Kinetics and Mechanism*, John-Wiley and Sons, New York, 1981. c) Bernasconi, C.F. *Relaxation Kinetics*, Academic Press, Inc., New York, 1976. d) Steinfeld, J.I.; Francisco, J.S.; Hase, W.L. *Chemical Kinetics and Dynamics*, Prentice-Hall, Inc., 1989.

2.) For reviews of selected aspects of ultrafast spectroscopy, see: a) Rosspeintner, A.; Lang, B.; Vauthey, E. *Ann. Rev. Phys. Chem.* **2013**, *64*, 247. b) Elliott, A.B.S.; Horvath, R.; Gordon, K.C. *Chem. Soc. Rev.* **2012**, *41*, 1929. c) McCusker, J.K. *Acc. Chem. Res.* **2003**, *36*, 876. d) Chen, L.X. *Ann. Rev. Phys. Chem.* **2005**, *56*, 221. e) Bressler, C.; Chergui, M. *Ann Rev. Phys. Chem.* **2010**, *61*, 263. f) Frontiera, R.R.; Fang, C.; Dasgupta, J.; Mathies, R.A. *Phys. Chem. Chem. Phys.* **2012**, *14*, 405. g) Anderson, N.A.; Lian, T.Q. *Ann. Rev. Phys. Chem.* **2005**, *56*, 491.

3.) a) Ballhausen, C.J. *Introduction to Ligand Field Theory*, McGraw-Hill, New York, 1962. b) Figgis, B.N.; Hitchman, M.A. *Ligand Field Theory and its Applications*, Wiley-VCH, New York, 2000.

4.) For examples of recent efforts in the computational studies of transition metal complexes, see: a) Kaduk, B.; Kowalczyk, T.; Van Voorhis, T. *Chem. Rev.* **2012**, *112*, 321. b) Tsipis, A.C. *Coord. Chem. Rev.* **2014**, *272*, 1. c) Jacob, C.R.; Reiher, M. *Int. J. Quant. Chem.* **2013**, *112*, 3661. d) England, J.; Scarborough, C.C.; Weyhermueller, T.; Sproules, S.; Wieghardt, K. *Eur. J. Inorg. Chem.* **2012**, 4605. e) Lin, Z.Y. *Acc. Chem. Res.* **2010**, *43*, 602. f) Bowman, D.N.; Jakubikova, E. *Inorg. Chem.* **2012**, *51*, 6011. g) Tsuchiya, T.; Shrestha, K.; Jakubikova, E. *J. Chem. Th. Comp.* **2013**, *9*, 3350. h) Olatunji-Ojo, O.A.; Cundari, T.R. *Inorg. Chem.* **2013**, *52*, 8106. i) Bossert, J.; Daniel, C. *Coord. Chem. Rev.* **2010**, *252*, 2493.

5.) a) Alstrum-Acevedo, J.H.; Brennaman, M.K.; Meyer, T.J. *Inorg. Chem.* **2005**, *44*, 6802. b) Karkas, M.D.; Johnston, E.V.; Verho, O.; Akermark, B. *Acc. Chem. Res.* **2014**, *47*, 100, and references therein. c) McConnell, I.; Li, G.; Brudvig, G.W. *Chem. Bio.* **2010**, *17*, 434. d) Balzani, V.; Credi, A.; Venturi, M. *ChemSusChem* **2008**, *1*, 26.

6.) Creutz, C.; Chou, M.; Netzel, T. L.; Okumura, M.; Sutin, N. *J. Am. Chem. Soc*. **1980**, *102*, 1309.

7.) For example, see: a) Hewitt, J.T.; Vallett, P.J.; Damrauer, N.H. *J. Phys. Chem. A* **2012**, *116*, 11536. b) Kaemper, S.; Paretzki, A.; Fiedler, J.; Zalis, S.; Kaim, W. *Inorg. Chem.* **2012**, *51*, 2097. c) Low, P.J.; Bock, S. *Electrochim. Acta* **2013**, *110*, 681. d) Gabrielsson, A.; Matousek, P.;

Towrie, M.; Hartl, F.; Zalis, S.; Vlcek, A. *J. Phys. Chem. A* **2005**, *109*, 6147. e) Marcaccio, M.; Paolucci, F.; Paradisi, C.; Carano, M.; Roffia, S.; Fontanesi, C.; Yellowlees, L.J.; Serroni, S.; Campagna, S.; Balzani, V. *J. Electro. Chem.* **2002**, *532,* 99. f) Jones, S.W.; Vrana, L.M.; Brewer, K.J. *J. Organomet. Chem.* **1998**, *554*, 29. g) Braterman, P.S.; Song, J.I.; Peacock, R.D. *Inorg. Chem.* **1992**, *31*, 555.

8.) McCusker, J. K.; Rheingold, A. L.; Hendrickson, D. N. *Inorg. Chem.* **1996**, *35*, 2100.

9.) Constable, E. C.; Cargill Thompson, A. M. W.; Tocher, D. A.; Daniels, M. A. M. *New J. Chem.* **1992**, *16*, 855.

10.) Caspar, J.; Meyer, T. J. *J. Am. Chem. Soc.* **1983**, *105*, 5583.

11.) Juban, E. A.; McCusker, J. K., *J. Am. Chem. Soc.* **2005,** 127, 6857.

12.) Brown, A.M.; McCusker, C.E.; Blanco-Rodriguez, A.M.; Towrie, M.; Clark, I.P.; Vlcek, A.; McCusker, J.K., submitted for publication.

13.) Juris, A.; Balzani, V.; Barigelletti, F.; Campagna, S.; Belser, P.; Von Zelewsky, A. *Coord. Chem. Rev.* **1988**, *84*, 85, and references therein.

14.) The degree to which ligand-localized absorptions will shift upon binding to a metal center will vary from system to system, however, for the purposes of the present discussion these changes are relatively small.

15.) Oh, D.H.; Boxer, S.G. *J. Am. Chem. Soc.* **1989**, *111*, 1130.

16.) Bradley, P.G.; Kress, N.; Hornberger, B.A.; Dallinger, R.F.; Woodruff, W.H. *J. Am. Chem. Soc.* **1981**, *103*, 7441.

17.) a) Damrauer, N.H.; Cerullo, G.; Yeh, A.; Boussie, T.R.; Shank, C.V.; McCusker, J.K. *Science* **1997**, *275*, 54. b) Yeh, A.T.; Shank, C.V.; McCusker, J.K. *Science* **2000**, *289*, 935. c) Wallin, S.; Davidsson, J.; Modin, J.; Hammarström, L. *J. Phys. Chem. A* **2005**, *109*, 4697. d) Cooley, L.F.; Bergquist, P.; Kelley, D.F. *J. Am. Chem. Soc.* **1990**, *112*, 2612. e) DeArmond, M.K.; Myrick, M.L. *Acc. Chem. Res.* **1989**, *22*, 364.

18.) a) McCusker, J.K; Walda, K.; Dunn, R.C.; Simon, J.D.; Magde, D.; Hendrickson, D.N. *J. Am. Chem. Soc.* **1993**, *115* , 298. b) Zhang, W.; Alonso-Mori, R.; Bergmann, U.; Bressler, C.; Chollet, M.; Galler, A.; Gawelda, W.; Hadt, R.G.; Hartsock, R.W.; Kroll, T.; Kjaer, K.S.; Kubicek, K.; Lemke, H.T.; Liang, H.Y.W.; Meyer, D.A.; Nielsen, M.M.; Purser, C.; Robinson, J.S.; Solomon, E.I.; Sun, Z.; Sokaras, D.; van Driel, T.B.; Vanko, G.; Weng, T.-C.; Zhu, D.; Gaffney, K.J.

Nature **2014**, *509*, 345. c) Cannizzo, A.; Milne, C.J.; Consani, C.; Gawelda, W.; Bressler, C.; van Mourik, F.; Chergui, M. *Coord. Chem. Rev.* **2010**, *254*, 2677, and references therein.

19.) Wang, X.Y.; Del Guerzo, A.; Schmehl, R.H. *J. Photchem. Photobiol. C* **2004**, *5*, 55.

20.) a) Horvath, R.; Gordon, K.C. *Coord. Chem. Rev.* **2010**, *254*, 2505. b) Butler, J.M.; George, M.W.; Schoonover, J.R.; Dattelbaum, D.M.; Meyer, T.J. *Coord. Chem. Rev,* **2007**, *251*, 492. c) Schoonover, J.R.; Strouse, G.F. *Chem. Rev.* **1998**, *98*, 1335. d) Blanco-Rodriguez, A.M.; Kvapilova, H.; Sykora, J.; Towrie, M.; Nervi, C.; Volpi, G.; Zalis, S. ; Vlcek, A., Jr. *J. Am. Chem. Soc.* **2014**, *136*, 5963. e) Dattelbaum, D.M.; Omberg, K.M.; Hay, P.J.; Gebhart, N.L.; Martin, R.L.; Schoonover, J.R.; Meyer, T.J. *J. Phys. Chem. A* **2004**, *108*, 3527. f) Curtright, A.E.; McCusker, J.K. *J. Phys. Chem. A* **1999**, *103*, 7032.

21.) A ligand-localized ππ* excited state will have absorption features reminiscent of the radical anion, but the spectral profiles are typically easy to differentiate. See ref 19 for further details.

22.) Smeigh, A.L.; Creelman, M.; Mathies, R.A.; McCusker, J.K. *J. Am. Chem. Soc.* **2008**, *130*, 14105.

23.) a) Chang, J.; Fedro, A.J.; van Veenendaal, M. *J. Chem. Phys.* **2012**, *407*, 65. b) Yoon, S.; Kukura, P.; Stuart, C.M.; Mathies, R.A. *Mol. Phys.* **2006**, *104*, 1275. c) Cannizzo, A.; van Mourik, F.; Gawelda, W.; Zgrablic, G.; Bressler, C.; Chergui, M. *Angew. Chem. Int. Ed.* **2006**, *45*, 3174. d) Bhasikuttan, A.C.; Suzuki, M.; Nakashima, S.; Okada, T. *J. Am. Chem. Soc.* **2002**, *124*, 8398.

24.) Vallett, P.J.; Damrauer, N.H. *J. Phys. Chem. A* **2013**, *117*, 6489, and references therein.

25.) Damrauer, N. H.; McCusker, J. K., *J. Phys. Chem. A.* **1999**, *103*, 8440.

26.) a) Monat, J. E.; McCusker, J. K. *J. Am. Chem. Soc*. **2000**, *122*, 4092. b) Juban, E.A.; Smeigh, A.L.; Monat, J.E.; McCusker, J.K. *Coord. Chem. Rev.* **2006**, *250*, 1783.

27.) For example, the widely used Grätzel cell sensitizer $Ru(dcbpy)_2(NCS)_2$ exhibits an irreversible $Ru^{2+/3+}$ oxidation wave in its cyclic voltammogram.

28.) The photophysics of Ru^{2+}-terpyridine complexes can be significantly influenced by the presence of ligand-field excited states at energies just above the lowest-energy ^{3}MLCT state. See ref 24 for further details on this point.

29.) A recent report by Goodson and co-workers (Yoon, Z.S.; Chan, Y.-T.; Li, S.; Newkome, G.R.; Goodson, III T. *J. Phys. Chem. B* **2010**, *114*, 11731) assigned ground-state recovery in $[Fe(terpy)_2]^{2+}$ as originating from the ^{3}MLCT state. We respectfully disagree with this assignment based on several considerations, including the spectral evolution illustrated in Figure 4, the

complete absence of the optical signature for $terpy^-$ in the differential spectra reported by Goodson and co-workers, as well as the lifetime of the excited state (ca. 5 ns) being consistent with expectations from non-radiative decay theory for a $^5T_2 \rightarrow {}^1A_1$ conversion. In addition, recent time-resolved x-ray measurements by Sundström and co-workers (Canton, S.E.; Zhang, X.; Daku, L.M.L.; Smeigh, A.L.; Zhang, J.X.; Liu, Y.; Wallentin, C.-J.; Attenkofer, K.; Jennings, G.; Kurtz, C.A.; Gosztola, D.; Warnmark, K.; Hauser, A.; Sundström, V. *J. Phys. Chem. C* **2014**, *118*, 4536) confirm that the structure of the long-lived excited state of $[Fe(terpy)_2]^{2+}$ exhibits metrics consistent with a ligand-field excited state.

30.) One caveat to this statement is that spectral shifting due to solvent dynamics and/or vibrational cooling in a given excited state can in principle give rise to an observed change in the sign of $\Delta\varepsilon$ if one is probing in the vicinity of an isosbestic point of the differential spectrum.

Figure Captions.

Figure 1. Electronic absorption spectra of $[Ru(terpy)_2]^{2+}$ in CH_3CN solution. *Top.* Ground state. *Middle.* Spectrum obtained following bulk electrolysis at ~ +1200 mV. *Bottom.* Spectrum obtained following bulk electrolysis at ~ –1750 mV.

Figure 2. Comparison of the experimental (solid red) and redox-based calculated (dotted blue) differential absorption spectra of $[Ru(terpy)_2]^{2+}$ in CH_3CN solution. The experimental spectrum was acquired at a delay of Δt = 5 ps following MLCT excitation at 485 nm. The calculated spectrum was obtained based on eq 5 using a value of η = 0.3 as the scaling factor.

Figure 3. Spectral progression of $[Fe(terpy)_2]^{2+}$ in acetonitrile during bulk electrolysis from the ground state spectrum (green) to the oxidized or reduced spectrum (red). *Top.* Oxidation at +950 mV. The inset shows an expanded view of absorption changes for λ > 600 nm. *Bottom.* Reduction at -1650 mV. See Experimental section for further details.

Figure 4. Differential electronic absorption spectra for $[Fe(terpy)_2]^{2+}$ in CH_3CN solution. *Top.* Progression of full spectral traces for delays ranging from Δt = 200 - 1500 fs following excitation at 560 nm. The inset shows an expanded view of the region near 400 nm that is diagnostic for the presence (and loss) of $terpy^-$ based on the spectroelectrochemical data shown in the bottom portion of Figure 3. *Bottom.* Comparison of the calculated (dotted black) and experimental differential absorption spectra of $[Fe(terpy)_2]^{2+}$ measured at Δt = 200 fs (solid green) and 1000 fs (solid red). The calculated spectrum was derived based on eq 5 and a scaling factor of η = 0.17.

Figure 5. Electronic absorption spectra of $[Ru(bpy)_3]^{2+}$ in CH_3CN solution. (a) Ground state. (b) Spectrum obtained following bulk electrolysis ~150 mV positive of the Ru^{2+}/Ru^{3+} oxidation wave. (c) Spectrum obtained following bulk electrolysis ~100 mV negative of the first bpy/bpy^- reduction wave. (d) Comparison of the experimental (solid black, Δt = 5

ps following MLCT excitation at 485 nm) and redox-based calculated (dotted blue; η = 0.3) differential absorption spectra of $[Ru(bpy)_3]^{2+}$.

Figure 6. Differential electronic absorption spectra for $[Fe(bpy)_3]^{2+}$ in CH_3CN solution. *Top.* Progression of full spectral traces for delays ranging from of Δt = 30 - 1000 fs following MLCT excitation at 485 nm. *Bottom.* Comparison of the calculated (dotted black) and experimental differential absorption spectra of $[Fe(bpy)_3]^{2+}$ measured at Δt = 30 fs (solid green) and 1000 fs (solid red). The calculated spectrum was derived based on eq 5 and a scaling factor of η = 0.17.

Figure 1

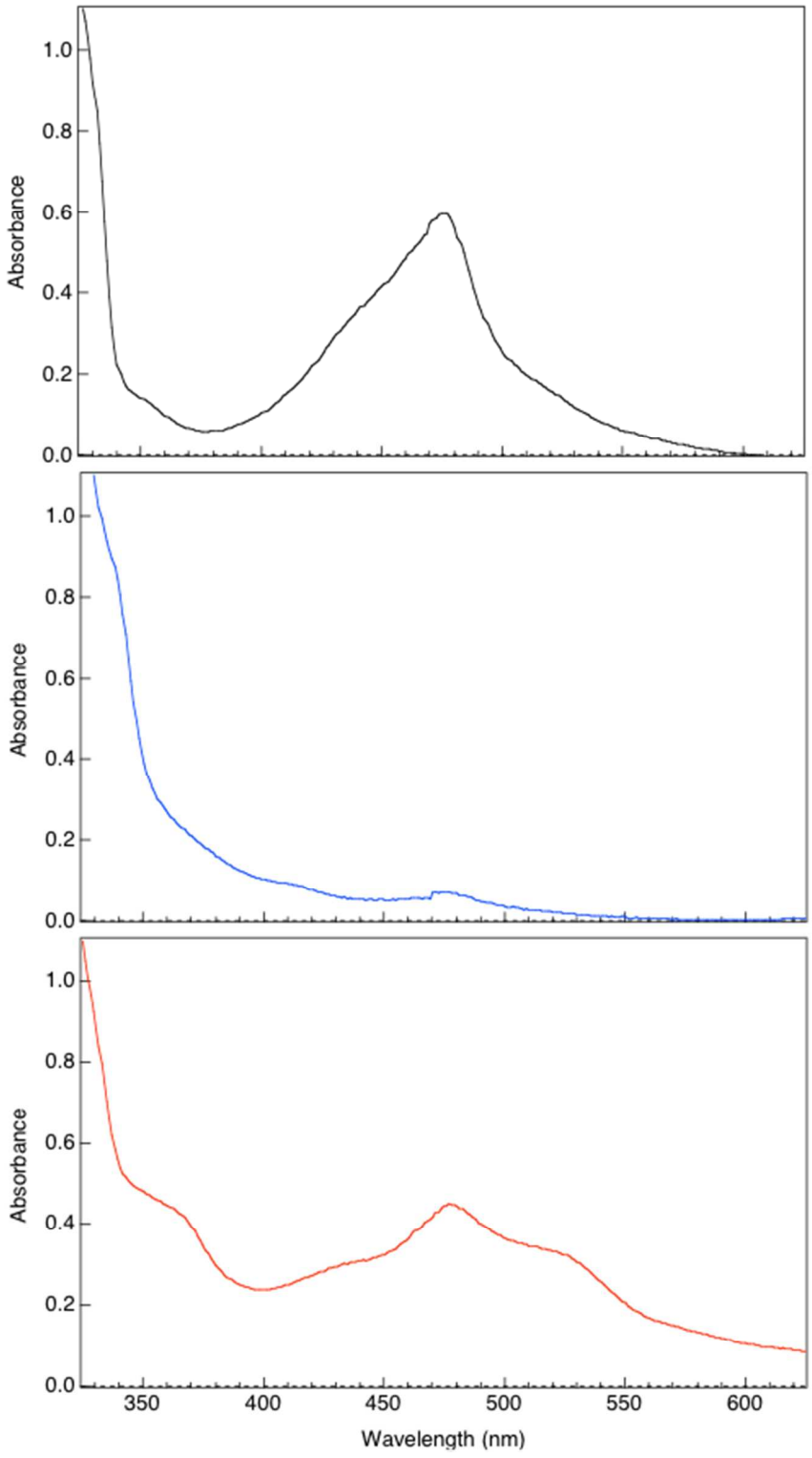
Absorbance
1.0
0.8
0.6
0.4
0.2
0.0
Absorbance
1.0
0.8
0.6
0.4
0.2
0.0
Absorbance
1.0
0.8
0.6
0.4
0.2
0.0
350
400
450
500
550
600
Wavelength (nm)

Figure 2

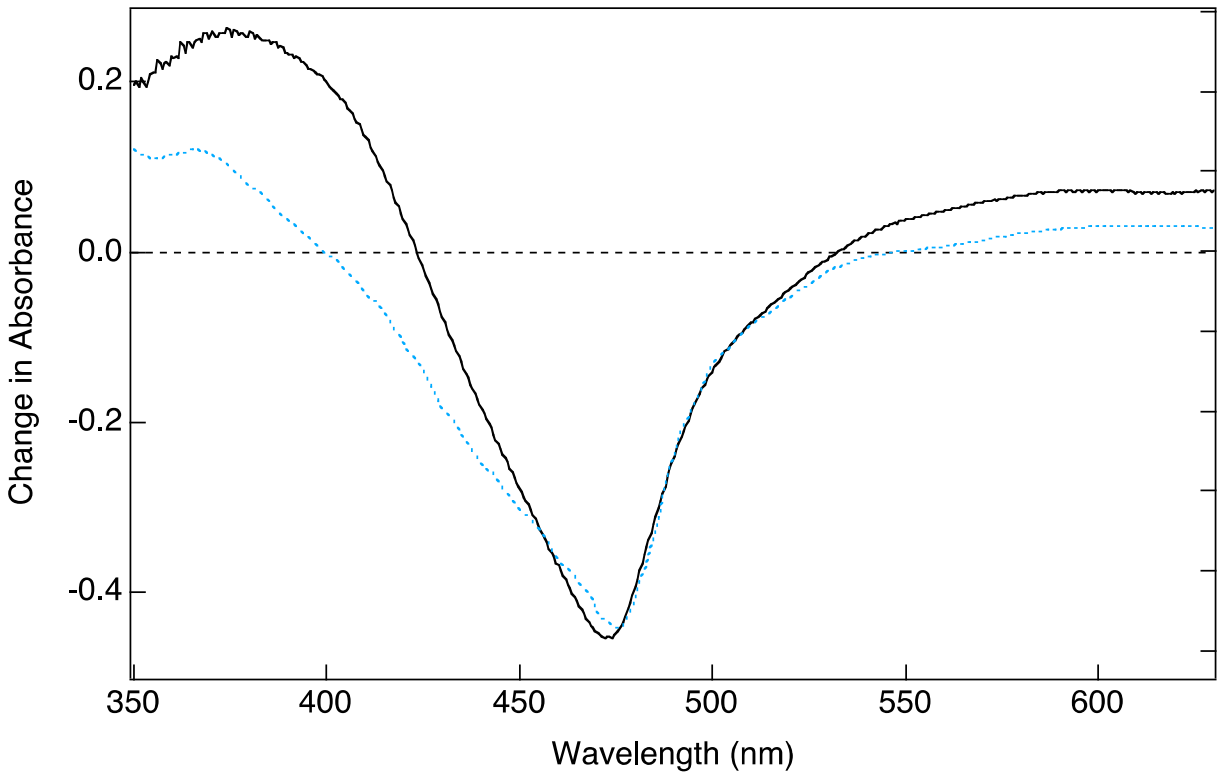
0.2
0.0
-0.2
-0.4
Change in Absorbance
350
400
450
500
550
600
Wavelength (nm)

Figure 3

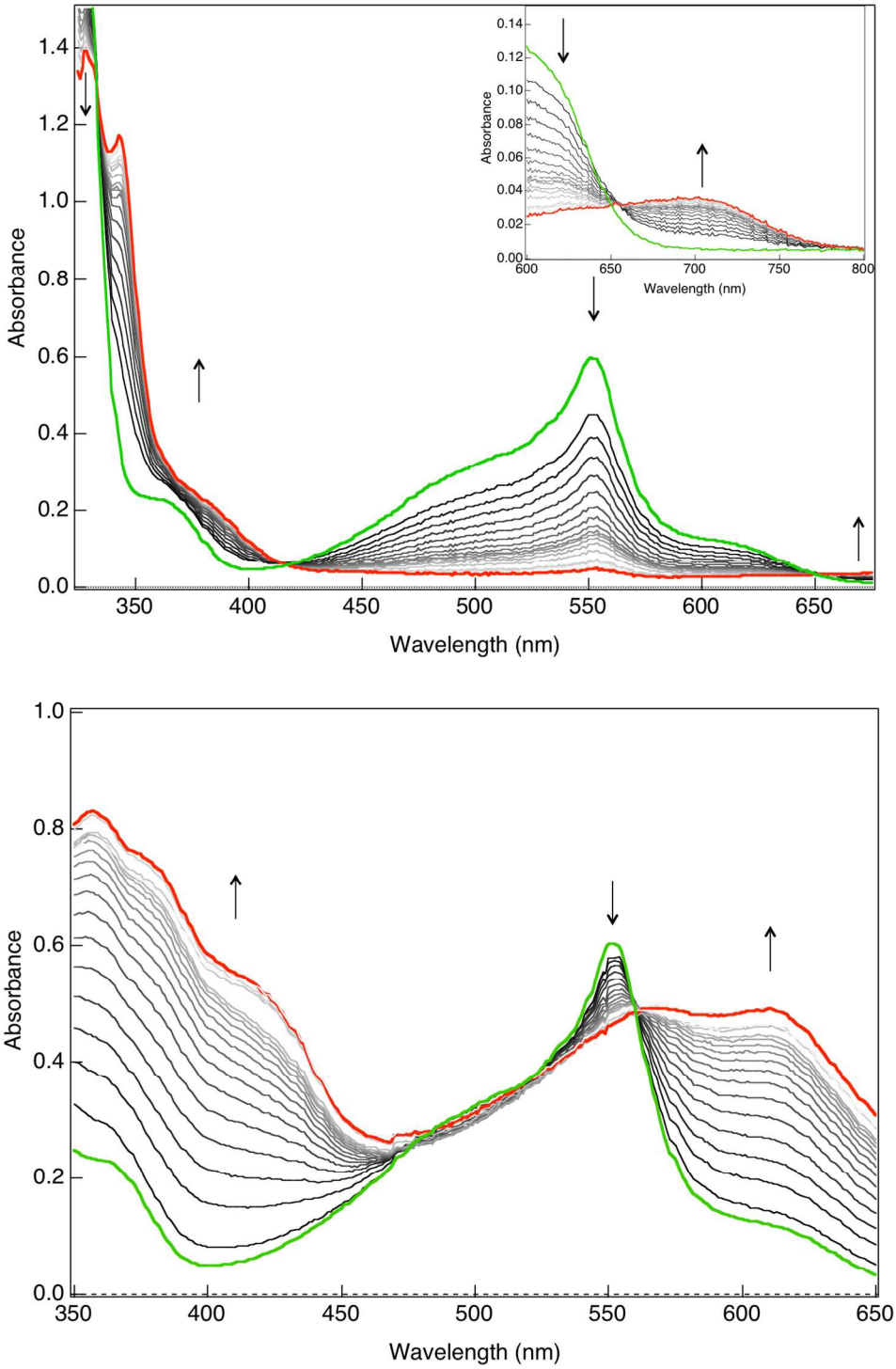
Absorbance
Wavelength (nm)
0.0
0.2
0.4
0.6
0.8
1.0
1.2
1.4
350
400
450
500
550
600
650
0.00
0.02
0.04
0.06
0.08
0.10
0.12
0.14
600
650
700
750
800

Figure 4

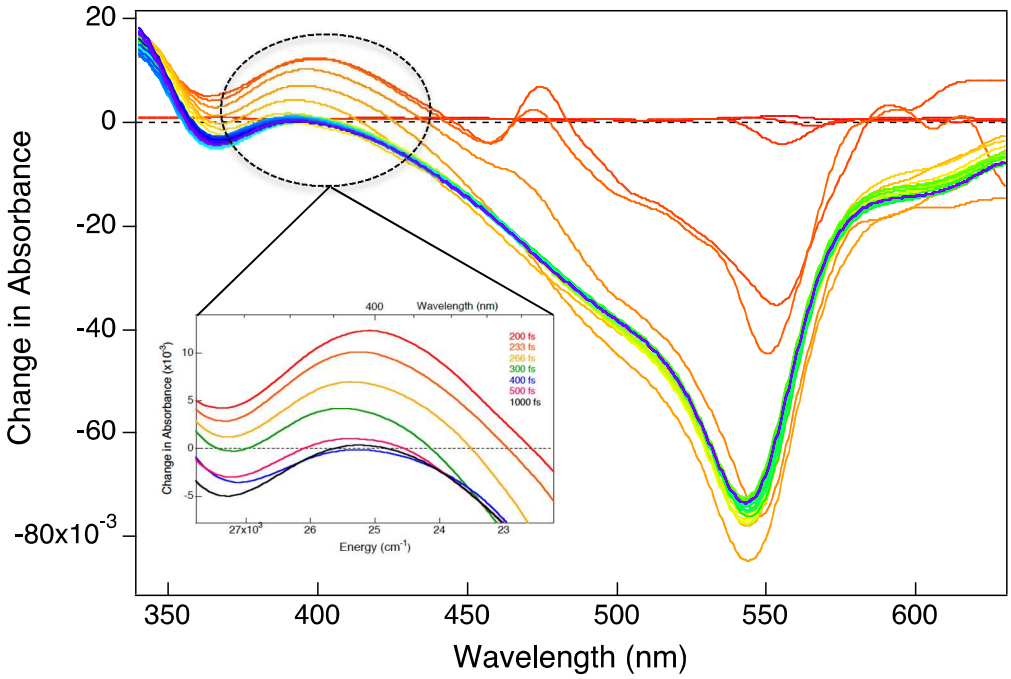
20
0
-20
-40
-60
-80x10-3
Change in Absorbance
350
400
450
500
550
600
Wavelength (nm)
400
Wavelength (nm)
200 fs
233 fs
266 fs
300 fs
400 fs
500 fs
1000 fs
Change in Absorbance (x10-3)
10
5
0
-5
27x10³
26
25
24
23
Energy (cm-1)

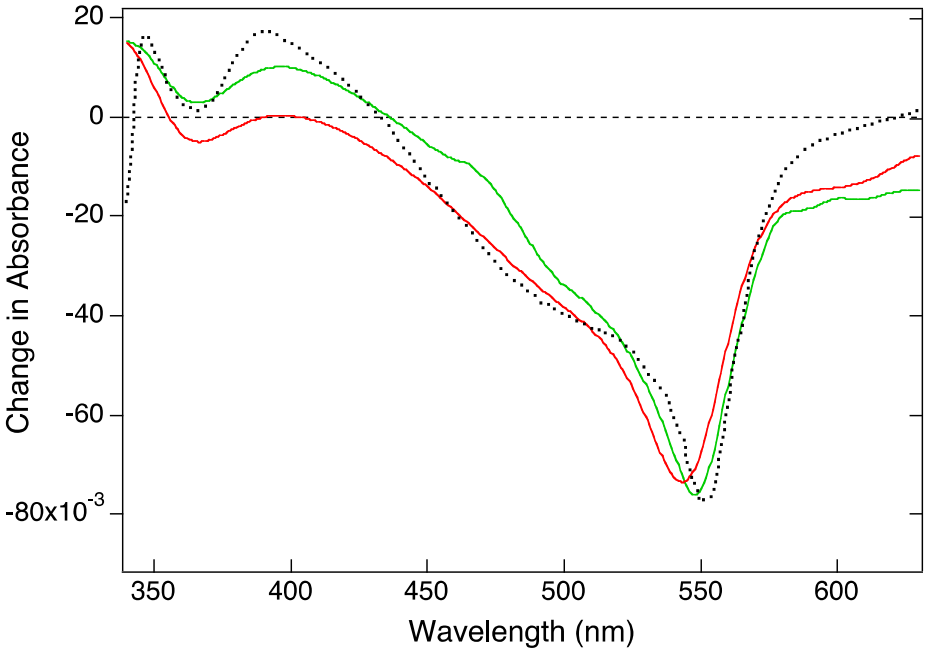
20
0
-20
-40
-60
-80x10-3
Change in Absorbance
350
400
450
500
550
600
Wavelength (nm)

Figure 5

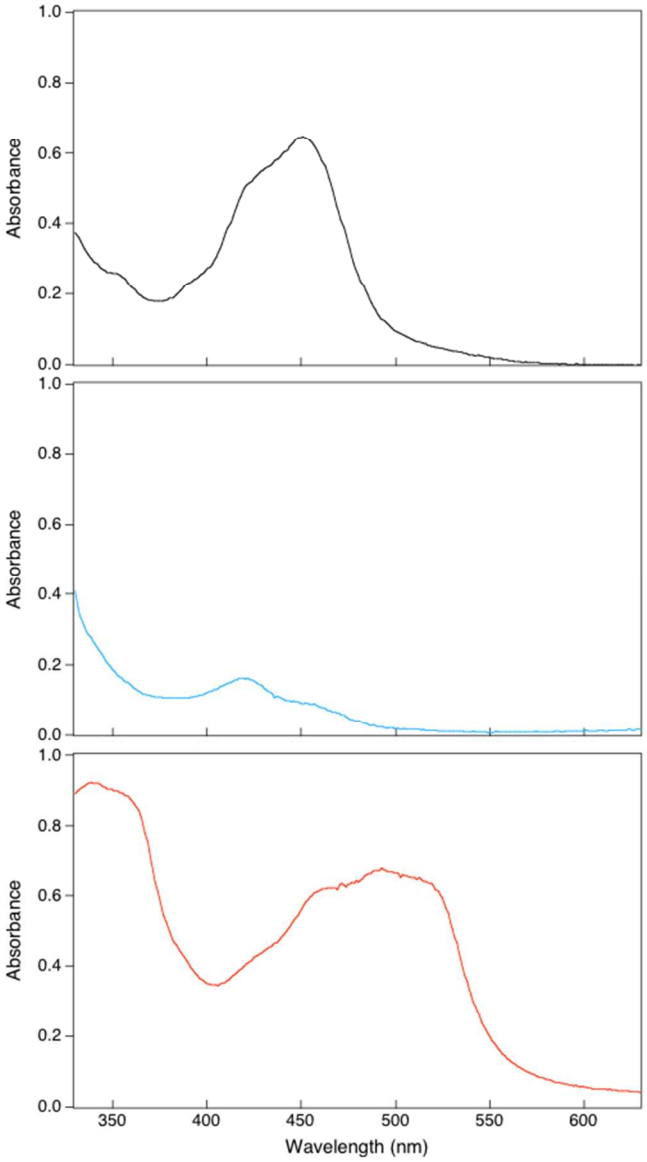
Absorbance
Absorbance
Absorbance
Wavelength (nm)
Change in Absorbance
Wavelength (nm)

Figure 6

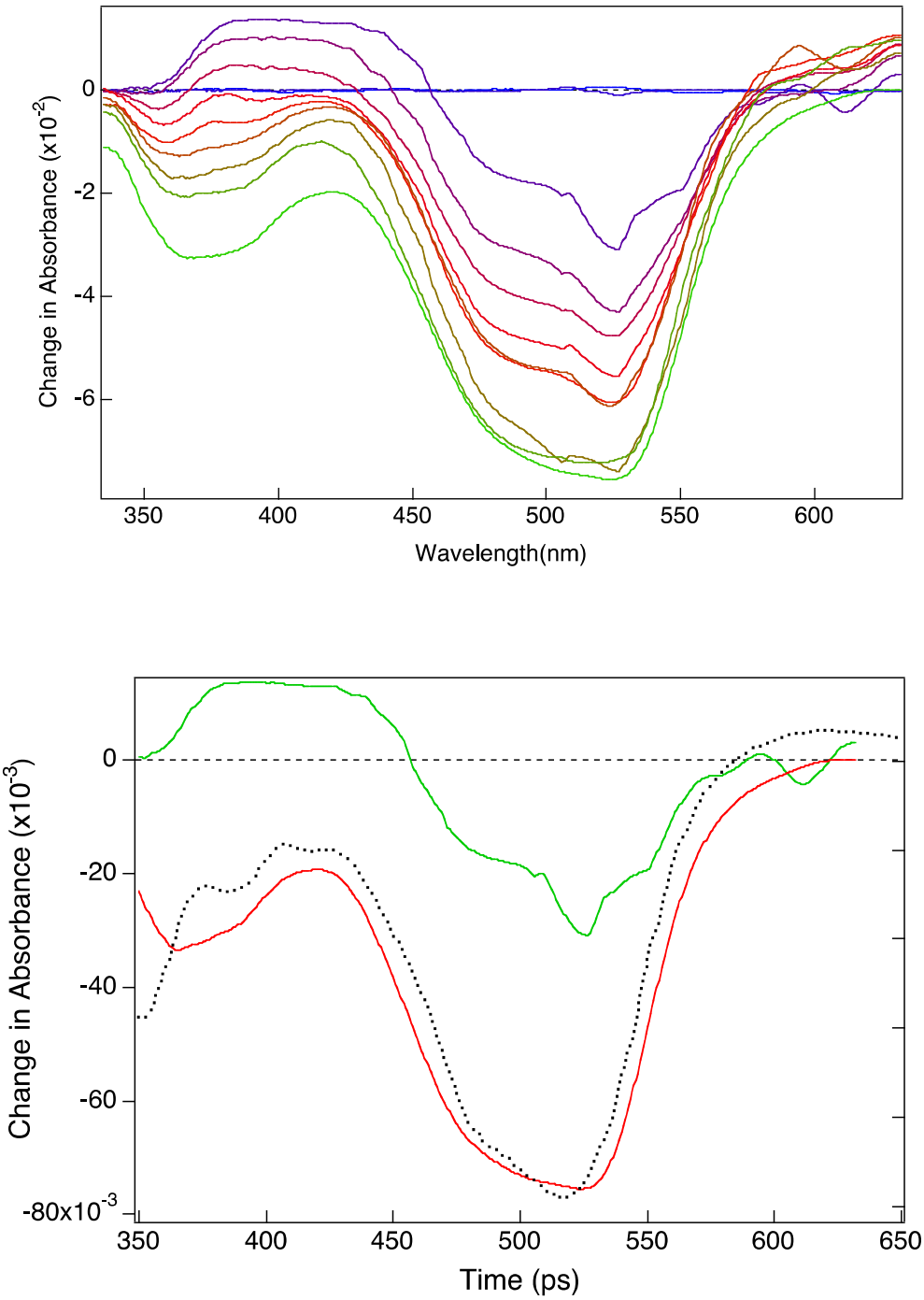
Change in Absorbance (x10-2)
0
-2
-4
-6
350
400
450
500
550
600
Wavelength(nm)
Change in Absorbance (x10-3)
0
-20
-40
-60
-80x10-3
350
400
450
500
550
600
650
Time (ps)

Scheme 1: Pictorial representation of the ground state, oxidized, reduced, and photo-excited versions of a $[M(terpy)_2]^{2+}$ chromophore. Several of the features anticipated in the MLCT excited state of the compound can be simulated using a combination of the spectra of the oxidized and reduced forms of the parent compound.

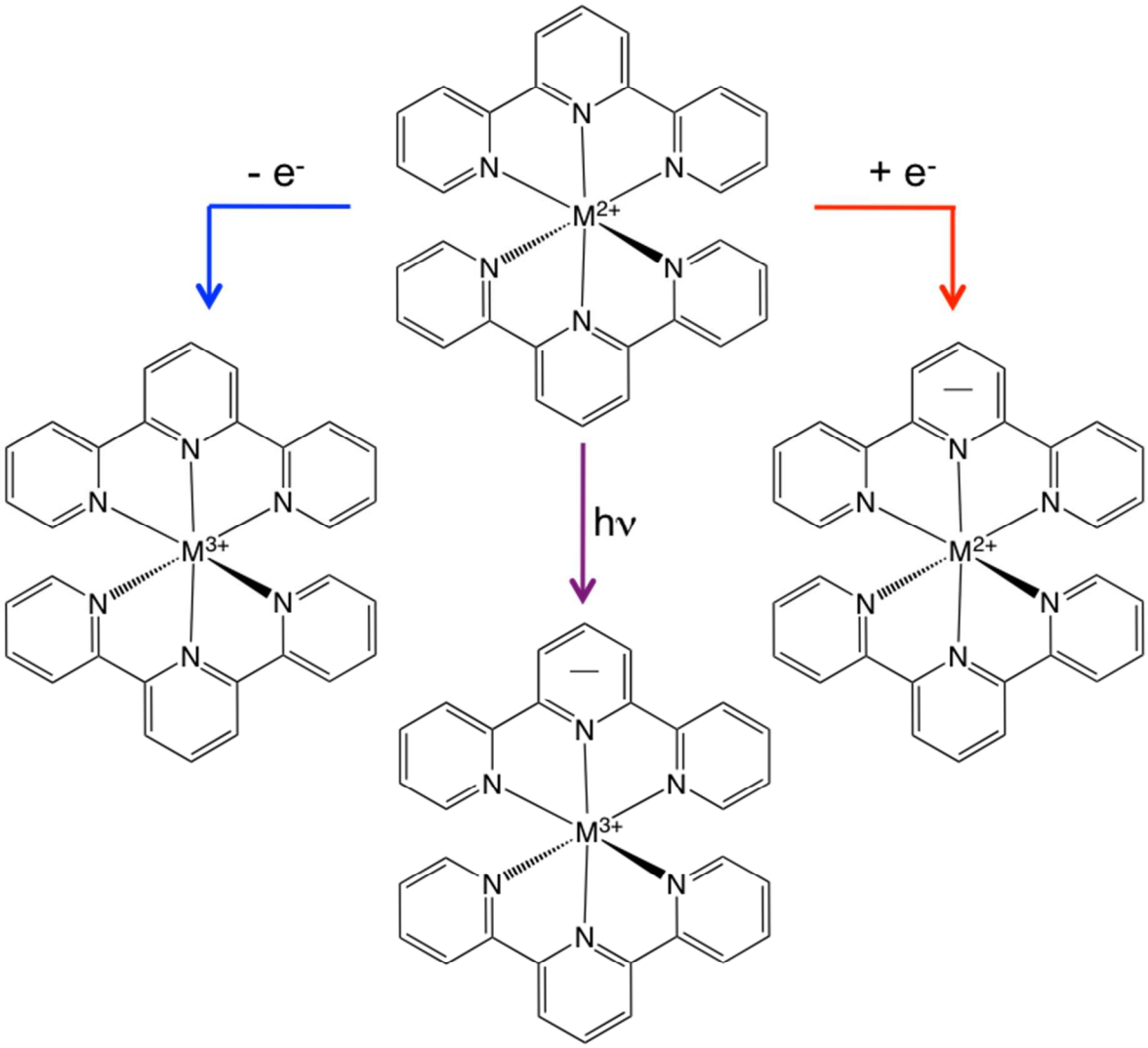

Table 1: Absorptive species present in the ground state, oxidized, and reduced forms of a $[M(L_1)(L_2)]^{2+}$ chromophore subject to the approximation that the spectra can be represented by a superposition of the various absorptive components present in each species. See text for further details.

	Ground State $[M(L_1)(L_2)]^{2+}$	Oxidized Species $[M(L_1)(L)_2]^{3+}$	Reduced Species $[M(L_1^-)(L_2)]^{+}$
Metal-localized (e.g., ligand-field bands)	M^{2+}	M^{3+}	M^{2+}
Ligand-localized (L_1)	L_1	L_1	L_1^-
Ligand-localized (L_2)	L_2	L_2	L_2
M-L_1 charge transfer (type)	M^{2+} - L_1 (MLCT)	M^{3+} - L_1 (LMCT)	M^{2+} - L_1^- (MLCT')
M-L_2 charge-transfer (type)	M^{2+} - L_2 (MLCT)	M^{3+} - L_2 (LMCT)	M^{2+} - L_2 (MLCT)

Table 2: Contributions to the differential MLCT excited-state absorption spectrum of a $[M(L_1)(L_2)]^{2+}$ species based on spectroelectrochemical data (ΔA_{ex}^{sim}) and what is expected experimentally (ΔA_{ex}^{exp}). Features that have a 1-to-1 correspondence between the two anticipated data sets are indicated in green, those that are overcompensated for in the redox-based approximation are highlighted in red, and species present in one spectrum that has no counterpart in the other are highlighted in blue. Positive and negative signs refer to absorptions and bleaches in the differential spectra, respectively.

	ΔA_{ex}^{sim}	ΔA_{ex}^{exp}
Ligand-localized $(L_1)^{loc}$	$+ L_1^-$ $- L_1$	$+ L_1^-$ $- L_1$
Charge-transfer $(M - L_1)^{LMCT}$	$+ (M^{3+} - L_1)$	$+ (M^{3+} - L_1^-)$
Charge-transfer $(M - L_2)^{LMCT}$	$+ (M^{3+} - L_2)$	$+ (M^{3+} - L_2)$
Charge-transfer $(M - L_1)^{MLCT}$	$+ (M^{2+} - L_1^-)$ $- (M^{2+} - L_1)$	$- (M^{2+} - L_1)$
Charge-transfer $(M - L_2)^{MLCT}$	$- (M^{2+} - L_2)$	$- (M^{2+} - L_2)$

Table 3: Contributions to the differential MLCT excited-state absorption spectrum of a $[M(L_1)(L_2)(L_3)]^{2+}$ species based on spectroelectrochemical data (ΔA_{ex}^{sim}) and what is expected experimentally (ΔA_{ex}^{exp}). Features that have a 1-to-1 correspondence between the two anticipated data sets are indicated in green, those that are overcompensated for in the redox-based approximation are highlighted in red, and species present in one spectrum that has no counterpart in the other are highlighted in blue. Positive and negative signs refer to absorptions and bleaches in the differential spectra, respectively.

	ΔA_{ex}^{sim}	ΔA_{ex}^{exp}
Ligand-localized $(L_1)^{loc}$	$+ L_1^-$ $- L_1$	$+ L_1^-$ $- L_1$
Charge-transfer $(M - L_1)^{LMCT}$	$+ (M^{3+} - L_1)$	$+ (M^{3+} - L_1^-)$
Charge-transfer $(M - L_2)^{LMCT}$	$+ (M^{3+} - L_2)$	$+ (M^{3+} - L_2)$
Charge-transfer $(M - L_3)^{LMCT}$	$+ (M^{3+} - L_3)$	$+ (M^{3+} - L_3)$
Charge-transfer $(M - L_1)^{MLCT}$	$+ (M^{2+} - L_1^-)$ $- (M^{2+} - L_1)$	$- (M^{2+} - L_1)$
Charge-transfer $(M - L_2)^{MLCT}$	$- (M^{2+} - L_2)$	$- (M^{2+} - L_2)$
Charge-transfer $(M - L_3)^{MLCT}$	$- (M^{2+} - L_3)$	$- (M^{2+} - L_3)$